Received: 7 July 2020 | Accepted: 18 November 2020

DOI: 10.1002/pamm.202000139

Parametric Study on Ridges Inducing Secondary Motions in Turbulent Channel Flow

Lars H. von Deyn[1,*], **Davide Gatti**[1], **Bettina Frohnapfel**[1], and **Alexander Stroh**[1]

[1] Institute of Fluid Mechanics (ISTM), Karlsruhe Institute of Technology (KIT), Kaiserstr. 10, 76131 Karlsruhe, Germany

A DNS parametric study of streamwise-aligned rectangular ridges is carried out in a fully developed turbulent channel flow with constant flow rate at $Re_b = 18000$. The simulations were carried out systematically varying the ridge height h, width w and structural wavelength S. The ridges generate a strong large-scale secondary motion, which is measured in terms of the integral swirl strength. Of the presented cases, the configuration with the ridge height $h = 0.1\,\delta$, $S/w = 4$, $S = 1\,\delta$ produces the strongest secondary flow of 4.5% U_b. The varying flow topology is discussed as a result of the varying ridge dimensions.

1 Introduction

Since the pioneering work of Hinze [1] it is known that spanwise inhomogeneous surface structures can lead to the formation of large-scale secondary motions of Prandtl's second kind. Recent studies show that these turbulent secondary flows alter important flow quantities such as the streamwise velocity and the skin-friction drag [2]. It is known that the secondary motion strength is strongly dependant on the spanwise structural wavelength S [3]. The present contribution presents a detailed parametric study of a channel flow with streamwise ridges, adding a systemic variation of the ridge geometry and the resulting flow topology to the present understanding of secondary flows over spanwise inhomogeneous surfaces.

2 Procedure

Direct numerical simulations (DNS) of a fully developed turbulent channel flow are carried out under a constant flow rate condition at $Re_b = 18000$ with $Re_b = \frac{U_b\,H}{\nu}$, U_b being the bulk velocity, H the channel height and ν the kinematic viscosity. The code implementation is based on a pseudo-spectral solver with Fourier expansions in the streamwise (x) and spanwise (z) directions and Chebyshev polynomials in the wall-normal direction (y) [4]. Periodic boundary conditions are applied for the velocity field in the streamwise and spanwise directions, while the wall-normal extension of the domain is bounded by no-slip boundary conditions at the lower and upper domain wall ($y = 0, 2\delta$). The numerical domain properties are listed in Table 1.

The wall structuring is modeled by an immersed boundary method (IBM) via the introduction of an external volume force field to the Navier-Stokes equations [5]. The ridge height h ($h = 0.025\,\delta$, $h = 0.05\,\delta$, $h = 0.075\,\delta$, $h = 0.1\,\delta$), width w ($S/w = 2$, $S/w = 4$) and structural wave length S (S=δ, $S = 2\,\delta$) as introduced in figure 1 are systematically varied. All combinations of the stated parameters were studied amounting to a total of 16 DNS simulations.

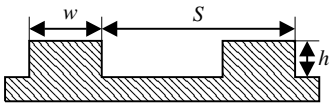

Fig. 1: Sketch of the studied ridge geometry.

$N_x \times N_y \times N_z$	$L_x \times L_y \times L_z$	$\Delta x^+ \times \Delta y^+_{min} \times \Delta z^+$
$768 \times 385 \times 384$	$8\,\delta \times 2\,\delta \times 4\,\delta$	$5.2 \times 0.02 \times 5.2$

Table 1: Numerical properties of the DNS.

3 Results

The skin friction coefficient C_f and the integrated swirling strength for all cases are presented in figure 2, yielding a good overview of the global flow properties. The skin friction coefficient is defined as $C_f = \frac{2\,\tau_w}{\rho\,U_b^2}$, τ_w being the wall shear stress and ρ the fluid density. The swirling strength is a good indication of the secondary motion strength and is defined as the imaginary part of the complex eigenvalue of the velocity gradient tensor λ_{ci} [6]. In figure 2, the extrinsic average of the dimensionless swirling strength is presented. The results indicate a correlation between C_f

* Corresponding author: e-mail von-deyn@kit.edu

and swirling strength, which both increase with increasing ridge height h. However, the cases depicted in orange ($S = \delta$ and $S/w = 4$) yield a relatively strong secondary motion at less increased C_f-values. This could be related to the different flow topology in these cases, of which visualisations are shown in figure 3 overlaid with the critical points.

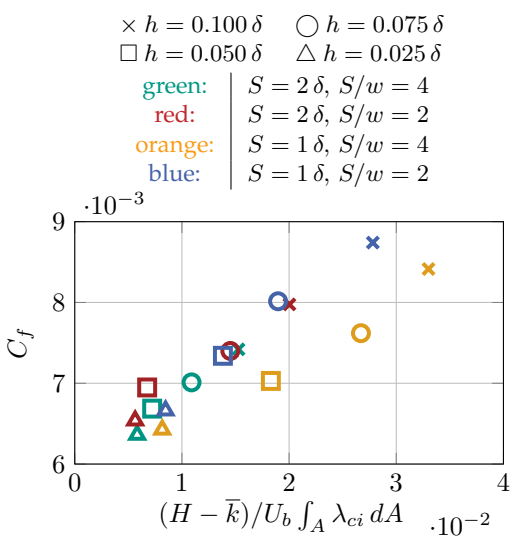

Fig. 2: C_f plotted against the extrinsic mean of the swirling strength (imaginary part of the complex eigenvalue of the velocity gradient tensor λ_{ci} [6]).

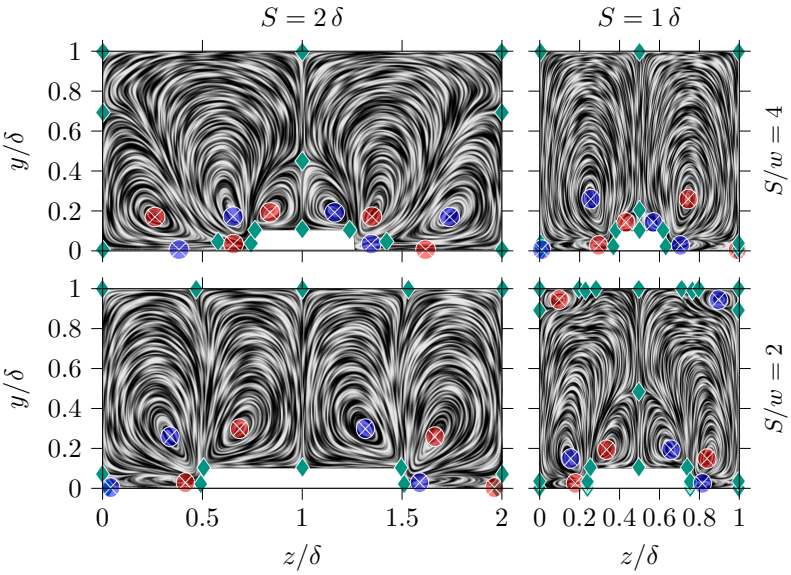

Fig. 3: LIC visualization of secondary motion overlaid with critical points for the cases with $h = 0.1\,\delta$. Green diamonds: (half-) saddles. Red circles: clockwise rotation nodes. Blue circles: anti-clockwise rotation nodes.

Here, green diamonds denote (half-) saddles, red circles clockwise rotation nodes and blue circles anti-clockwise rotation nodes. From the visualisations a distinct upward motion at the ridge corners can be observed for all cases. Recent studies show that the secondary motion is linked to the velocity deflection at the ridge corners [7]. Although the upward motion at the corners is present in all cases, the flow topology varies strongly. The case with the strongest secondary motion (4.5% U_b) $S = \delta$ and $S/w = 4$ (top right corner of figure 3) is dominated by two counter-rotating vortex pairs. The upward motion spans over the width of the ridge giving rise to a secondary motion extending to the channel core region. Two small vortex pairs are present, one located left and right of the ridge and one in direct vicinity on the ridge, which do not significantly contribute to the secondary flow. For the remaining cases $S/w = 2$ (bottom row of figure 3) and $S = 2\,\delta$, $S/w = 4$ (top left of figure 3) these two vortex pairs grow significantly, altering the flow topology and weakening the integral strength of the secondary motion (approx. 0.5% U_b weaker). Comparing $S/w = 2$ and $S/w = 4$ for $S = 1$ (right column of figure 3), it can bee seen that the vortex pair on the ridge is significantly larger for $S/w = 2$ due to the wider ridge width and thus greater spatial distance of the ridge edges generating the upward motion.

In conclusion, a spanwise narrow ridge with a structural wavelength of $S \approx \delta$ gives rise to the strongest secondary motion (4.5% U_b), which is in agreement with the available literature [2,3,7]. The present study indicates that the secondary motion is strongest in case of a geometry giving rise to a single counter-rotating vortex pair. Hereby, the increase in friction cannot solely be explained with the increase in wetted surface area [8]. With increasing complexity of the flow topology, i.e. size and number of the vortex structures in the ridge vicinity, the integral secondary motion strength decreases and the friction losses increase. If strong secondary currents are desired while minimizing the friction losses, a spanwise narrow, high-protruding ridge-like structure seems to be favorable.

Acknowledgements This work is supported by the Priority Programme SPP 1881 Turbulent Superstructures of the Deutsche Forschungsgemeinschaft. This work was performed on the supercomputer ForHLR Phase II and the storage facility LSDF funded by the Ministry of Science, Research and the Arts Baden-Württemberg and by the Federal Ministry of Education and Research.
Open access funding enabled and organized by Projekt DEAL.

References

[1] J. O. Hinze, The Physics of Fluids **10**(9), S122–S125 (1967).
[2] T. Medjnoun, C. Vanderwel, and B. Ganapathisubramani, Journal of Fluid Mechanics **886**(March), A31 (2020).

[3] D. D. Wangsawijaya, R. Baidya, D. Chung, I. Marusic, and N. Hutchins, Journal of Fluid Mechanics **894**(July) (2020).
[4] M. Chevalier, P. Schlatter, A. Lundbladh, and D. S. Henningson, SIMSON: A Pseudo-Spectral Solver for Incompressible Boundary Layer Flows (Mekanik, Kungliga Tekniska högskolan, Stockholm, 2007).
[5] D. Goldstein, R. Handler, and L. Sirovich, Journal of Computational Physics **105**(2), 354–366 (1993).
[6] J. Zhou, R. J. Adrian, S. Balachandar, and T. M. Kendall, Journal of Fluid Mechanics **387**(May), 353–396 (1999).
[7] A. Stroh, K. Schäfer, B. Frohnapfel, and P. Forooghi, Journal of Fluid Mechanics **885**(February) (2020).
[8] D. Gatti, L. von Deyn, P. Forooghi, and B. Frohnapfel, Experiments in Fluids **61**(3), 81 (2020).

